Research Article | Vol. 29, No. 25 / 6 Dec 2021 / Optics Express 41798
Optics EXPRESS

Sub-terahertz bandwidth capactively-loaded thin-film lithium niobate electro-optic modulators based on an undercut structure

XUECHENG LIU, BING XIONG,* CHANGZHENG SUN, JIAN WANG, ZHIBIAO HAO, LAI WANG, YANJUN HAN, HONGTAO LI, AND YI LUO

Beijing National Research Center for Information Science and Technology (BNRist), Department of Electronic Engineering, Tsinghua University, Beijing 100084, China
*bxiong@tsinghua.edu.cn

Abstract: A thin film lithium niobate (TFLN) electro-optic modulator based on a partially removed benzocyclobutene (BCB) bonding layer is proposed for sub-terahertz bandwidth. Low-loss microwave transmission is realized by periodic capacitively loaded travelling-wave electrodes (CL-TWEs) with an undercut structure, and the air-filled region beneath the modulator arms is adjusted to secure impedance and velocity matching. A low half-wave voltage length product of 1.2 V·cm can be achieved with 2-μm-gap loaded electrodes, while the 3-dB electro-optic modulation bandwidth for 10 mm modulation length is estimated beyond 300 GHz, thus allowing sub-terahertz operation.

1. Introduction

With the increasing demand of data transmission rate, wide bandwidth electro-optic modulators are required in 5G communications and beyond [1]. Modulators based on silicon or III-V semiconductors are difficult to break the bandwidth limitation due to high microwave loss [2,3]. Lithium niobate with high insulation and low dielectric loss has been targeted for ultra-wide bandwidth modulators [4,5]. Furthermore, the high index contrast of waveguides on ion-sliced thin-film lithium niobate (TFLN) allows a narrow electrode gap, thus greatly reducing the half-wave voltage [6–17].

Traveling-wave electrodes are widely adopted in high-speed electro-optic modulators [2–17]. Coplanar waveguide traveling-wave electrodes (CPW-TWEs) are employed in most TFLN modulators [6–14], which allows a parallel push-pull configuration. To achieve wide modulation bandwidth, velocity matching between microwave and optical signals as well as impedance matching should be satisfied. As revealed by Fig. 1, narrow-gap electrodes are employed in TFLN modulators with high-contrast waveguide [6–17] for improved modulation efficiency. Meanwhile, a narrow signal electrode has to be employed to maintain a standard impedance of 50 Ω, thus increasing the surface resistance of the transmission line and leading to enhanced microwave loss. To overcome the modulation bandwidth limitation of CPW-TWEs due to the high microwave loss caused by narrow-gap electrodes, periodic capacitively-loaded travelling-wave electrodes (CL-TWEs) are adopted in TFLN modulators [15–17]. As illustrated in Fig. 1, CL-TWEs contain narrow-gap T-rails loaded between wide-gap CPW-TWEs to enhance the electric field intensity. As the T-rails act as capacitance loading and contribute little to the axial current [18], the capacitance and inductance per unit length of the CL-TWEs can be adjusted relatively independently by the loaded and unloaded elements. Low-loss microwave transmission can be realized with a wide unloaded signal electrode, while impedance matching can be maintained by increasing the gap between the unloaded signal and ground electrodes, shown as the dashed line on the right of Fig. 1. Consequently, high electric field loading efficiency and low microwave

#442091 https://doi.org/10.1364/OE.442091
Journal © 2021 Received 2 Sep 2021; revised 24 Oct 2021; accepted 23 Nov 2021; published 1 Dec 2021

Optics EXPRESS

loss can be secured simultaneously by employing CL-TWEs with narrow-gap T-rails and wide central signal electrode.

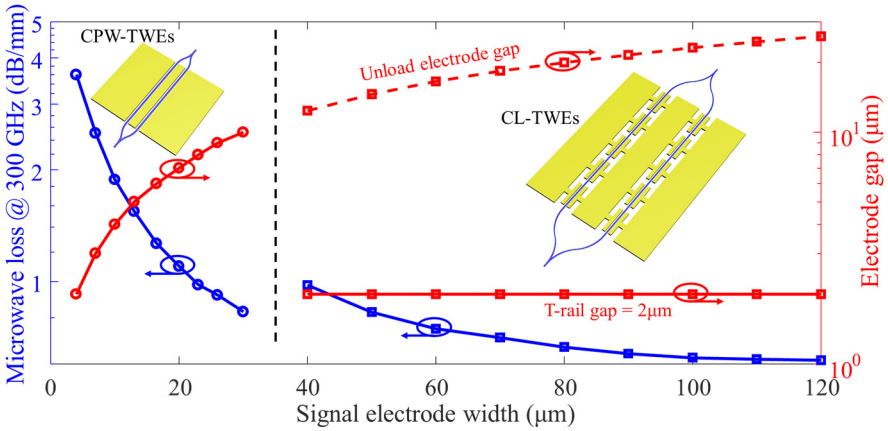

Fig. 1. Comparison of electrode gap and microwave loss between CPW-TWEs and CL-TWEs. The characteristic impedances of both structures are assumed to be 50 Ω.

However, as the capacitive loading also slows down the microwave signal, velocity matching is difficult to be satisfied with a relatively fast light wave in lithium niobate ($\varepsilon_{opt} \sim 5, \varepsilon_{RF} \sim 28$). The characteristic impedance Z_m and microwave refractive index n_m of CPW-TWEs can be expressed as follows [19]:

$$Z_m = \sqrt{\frac{L_0}{C_0}} \tag{1}$$

and

$$n_m = \frac{c}{v_m} = c\sqrt{L_0 C_0} \tag{2}$$

where C_0 and L_0 are the capacitance and inductance per unit length, and c is the speed of light in vacuum. On the other hand, as the T-rails mainly play a role of capacitive loading, the characteristic impedance Z'_m and microwave refractive index n'_m of the CL-TWEs can be estimated by [19]:

$$Z'_m = \sqrt{\frac{L_0}{C'_0}} = \sqrt{\frac{L_0}{C_0 + C_T}} \tag{3}$$

and

$$n'_m = \frac{c}{v'_m} = c\sqrt{L_0 C'_0} = c\sqrt{L_0(C_0 + C_T)} \tag{4}$$

where C_T represents the capacitance introduced by the T-rails, which leads to reduced characteristic impedance and microwave velocity. To secure impedance and velocity matching, it is essential to reduce the equivalent dielectric constant of the materials under the CL-TWEs for a reduced capacitance.

In previous reports, TFLN on quartz substrate instead of silicon substrate proved to be a possible solution [15–17]. To reduce the half-wave voltage length product $V_\pi L$, electrode gaps of 2 μm or even narrower are employed [10,15], resulting in further reduced microwave velocity and characteristic impedance due to an overloaded capacitance. Here we report using undercut structure to realize velocity and impedance matching in TFLN modulators based on CL-TWEs with narrow T-rail gaps.

Optics EXPRESS

2. Device structure

As shown in Fig. 2(a), air-filled undercut regions are formed beneath the TFLN modulation arms by partially removed photosensitive benzocyclobutene (BCB), which acts as the bonding layer and can be conveniently patterned by photolithography. The capacitance of CL-TWEs can be adjusted by varying the thickness of the BCB/air bonding layer. Consequently, the T-rail gap can be reduced while maintaining velocity and impedance matching, resulting in an improved bandwidth-voltage performance.

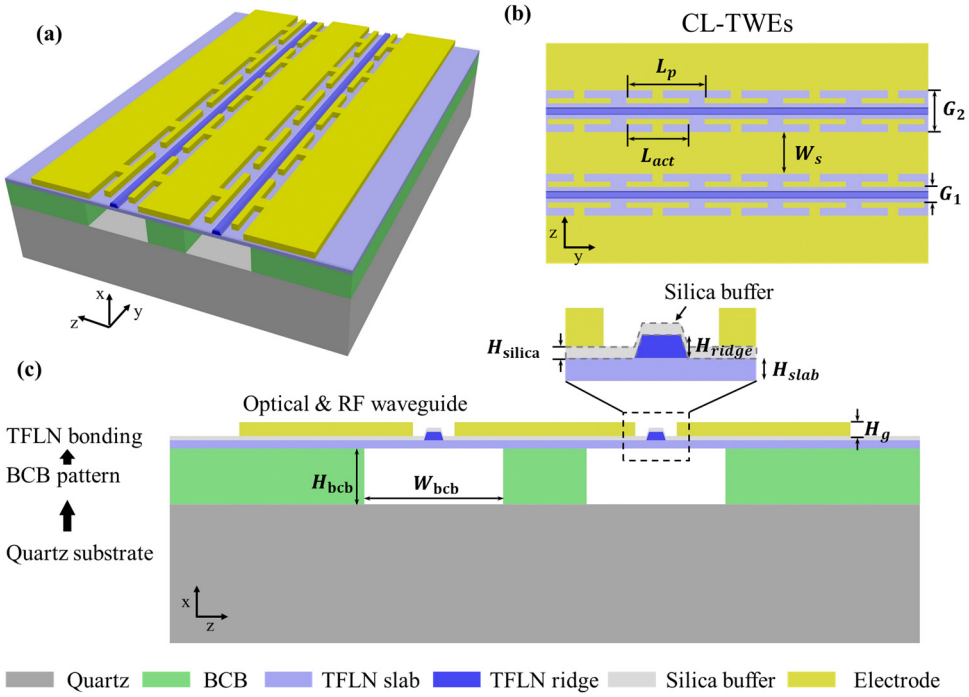

Fig. 2. (a) 3-D diagram of the proposed TFLN modulator, (b) top-view of the CL-TWEs, and (c) cross-section view of the modulation region. The modulation arms are aligned to the air-filled undercut region.

As shown in Fig. 2(c), the pattern of BCB bonding layer is defined by photolithography on the quartz substrate with low dielectric constant. Ion-sliced lithium niobate thin film is then bonded to the BCB layer. The optical waveguides as well as the T-rails of the CL-TWEs are formed over the air-filled region. Furthermore, the electrodes are separated from the TFLN slab by a thin silica buffer layer to ensure low optical absorption [15,17]. This configuration allows precise adjustment of the thickness and the width of the undercut region, so as to achieve the desired capacitance for CL-TWEs to maximize modulation bandwidth.

According to Eqs. (3) and (4), the microwave refractive index of the CL-TWEs can be related to the capacitance per unit length as follows:

$$n'_m = C'_0 \cdot c \cdot Z'_m \tag{5}$$

where Z'_m=50 Ω under the impedance matching condition. As the inductance can be adjusted flexibly by unloaded electrode spacing without deteriorating the half-wave voltage, the microwave index is found to depend solely on the capacitance of the CL-TWEs. A narrow T-rail gap

Optics EXPRESS

helps enhance the modulation electric field and reduce the half-wave voltage, but the increased capacitance slows down the microwave signal and limits the modulation bandwidth. To overcome this problem, the modulation arms are formed over the air-filled undercut regions, where the electric field is concentrated, as illustrated in Fig. 3(a). The effect of the undercut on the capacitance per unit length is shown in Fig. 3(b). The capacitance can be reduced by more than 20% to the desired value by adjusting the thickness of the BCB/air bonding layer. Thus both velocity and impedance matching can be achieved simultaneously with narrow-gap T-rails. The effect of velocity/capacitance mismatch on the modulation bandwidth is plotted in Fig. 3(c). For a device with 10 mm modulation length, a modulation bandwidth exceeding 300 GHz can be secured with less than 2% capacitance/index deviation, assuming lossless microwave transmission and perfect impedance matching. It is evident that in the proposed structure, the capacitance of narrow-gap CL-TWEs can be effectively reduced and precisely adjusted to attain a sub-terahertz modulation bandwidth.

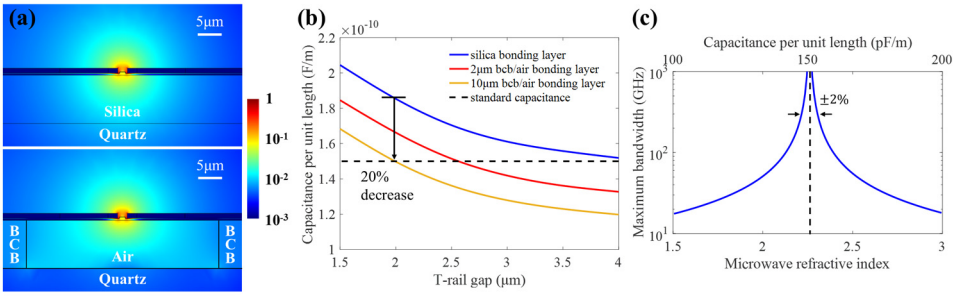

Fig. 3. (a) Normalized electric field with and without undercut. (b) Variation of the capacitance with the T-rail gap for different bonding layer thickness. (c) Modulation bandwidth varies with index/capacitance mismatch, assuming lossless microwave transmission and perfect impedance matching.

3. Design method and result

3.1. Design of the CL-TWEs

To ensure desirable modulation performance, the capacitance and inductance of the travelling-wave electrodes should be adjusted to ensure impedance and velocity matching. For CL-TWEs, the capacitance mainly comes from the narrow-gap T-rails, while their influence on the inductance is negligible. As a result, the capacitance and the inductance of the transmission line can be tuned separately by adjusting the loaded and unloaded elements. Through a full-wave simulation as shown in Fig. 4(a), for a TFLN modulator with silica bonding layer, the duty cycle of T-rails reduces with the electrode gap to maintain a constant capacitance. This would reduce the effective modulation length and increasing the half-wave voltage of the modulator. On the other hand, a narrow T-rail gap with a duty cycle of 90% can be secured for the undercut TFLN modulator by adjusting the BCB/air bonding layer thickness, thus achieving low half-wave voltage without degrading the microwave transmission. According to our simulations, a 2-μm T-rail gap with 90% duty cycle can be implemented with 10-μm-thick and 40-μm-wide undercut area beneath the two modulation arms. Meanwhile, the inductance can be adjusted by varying the dimensions of the unloaded electrodes. A wide central signal electrode is preferable as it helps reduce conductor loss, while the gap between the unloaded electrodes should be increased accordingly for constant inductance. However, the microwave loss due to T-rails increases as the connection region lengthens, and the radiation loss also increase as the signal electrode widens [20]. Consequently,

Optics EXPRESS

a signal electrode width of 120 μm together with an unloaded electrode gap of 26 μm are chosen to ensure low-loss microwave transmission as shown in Fig. 4(b). Furthermore, the influence of undercut region dimensions on microwave loss are also shown in the Figs. 4(c) and 4(d).

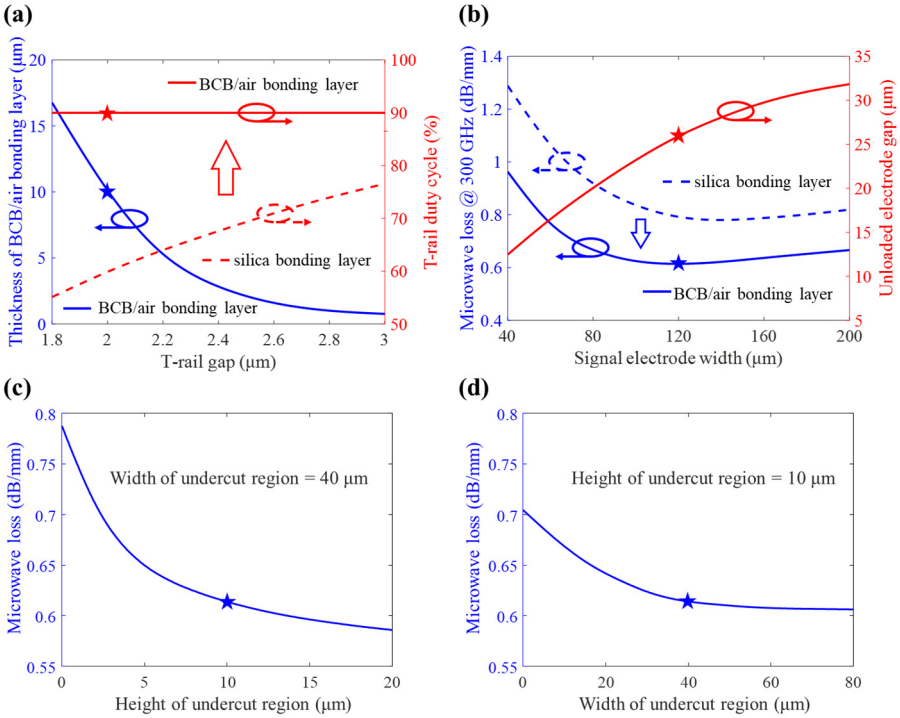

Fig. 4. (a) Variation of the T-rail gap with duty cycle to maintain a constant capacitance. A large duty cycle of 90% can be achieved by varying the BCB/air bonding layer thickness. (b) Variation of unloaded electrode gap and microwave loss with the width of the unloaded signal electrode under inductance matching condition. Microwave loss varies with the (c) height and (d) width of undercut area. The stars in (a), (b), (c) and (d) indicate the designed values.

As shown in Fig. 5, the microwave refractive index and microwave loss increase sharply close to the cut-off frequency (Bragg frequency) of the periodic CL-TWEs, which is inversely proportional to the electrode period [3]. To ensure a smooth variation of the microwave refractive index as well as a low microwave loss up to 300 GHz, CL-TWEs with a 20-μm T-rail period is chosen.

The optimized parameters for the TFLN modulator based on undercut structure are given in Table 1.

Table 1. Structural parameters of the TFLN modulator.

Parameters	L_p	L_{act}	W_s	G_1	G_2	H_g	W_{bcb}	H_{bcb}	H_{slab}	H_{ridge}	H_{silica}
Value (μm)	20	18	120	2	26	1	40	10	0.3	0.3	0.15

3.2. *Half-wave voltage*

The 2-μm-gap T-rails, which play an important role in the reduction of half-wave voltage, are separated from the TFLN by a 150-nm-thick silica buffer layer to maintain a low optical absorption

Optics EXPRESS

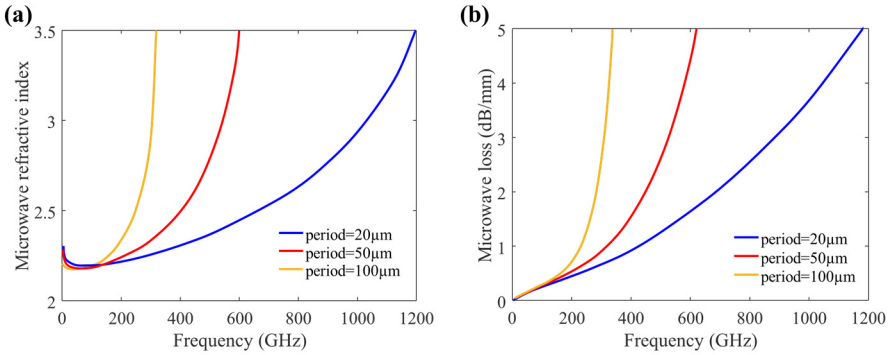

Fig. 5. The influence of cut-off frequency on (a) microwave refractive index and (b) microwave loss.

under 1 dB/cm [15], resulting in an on-chip loss less than 1 dB for 10 mm modulation length. The refractive index change of the X-cut TFLN modulator shown in Fig. 2 can be estimated as [21]:

$$\Delta n_{eff} = \frac{\iint_{LN} r_{33} E_e(x,z) \cdot |E_o(x,z)|^2 dxdz}{2 \iint |E_o(x,z)|^2 dxdz} \frac{n_{LN}^4}{n_{eff}} \tag{6}$$

where n_{LN} and r_{33} are the refractive index and the electro-optic coefficient of lithium niobite, while E_e and E_o are the modulation electric field and the optical field, respectively. And n_{eff} is the effective refractive index of the optical waveguide. 3D electric field together with optical mode are calculated by FEM to determine the half-wave voltage of the modulator. The electric field under 1 V applied voltage is shown in Fig. 6(a).

The refractive index variation along the optical waveguide are shown in Figs. 6(c) and 7(d). Due to the small period (20 μm) and the large duty cycle (90%) of the T-rails, strong fringing electric field exists between adjacent T-rails and attributes to the modulation. The average refractive index change is shown as the red line. Compared with conventional TFLN on silica bonding layer, the proposed TFLN modulator with air-filled undercut region exhibits a refractive index change enhancement of about 10%, thanks to the more concentrated optical confinement. For the under-cut TFLN with parameters given in Table 1, the half-wave-voltage length product is estimated to be as low as 1.2 V·cm.

3.3. Frequency response

The microwave S-parameters of the CL-TWEs obtained by finite element method (FEM) with surrounding ground-ring excitation [22] and radiation boundary are plotted in Fig. 7(a). Furthermore, the experimental and simulation data of our previous work [17] are also included in Fig. 7(a) for comparison. The extracted microwave refractive index in Fig. 7(b) shows a perfect match with the optical group index (~2.26). The microwave loss shown in Fig. 7(c) comes from three parts: Conductor loss dominates in the designed operating frequencies, which comes from the main electrodes and the T-rails, radiation loss shows a sharp increase at higher frequencies, while dielectric loss is relatively small for materials with low loss tangent, e.g. silica/quartz ($<2\times10^{-3}$) [23], BCB ($<10^{-2}$) [24] and lithium niobate ($<10^{-2}$) [25]. As a rough estimation, the 3-dB electro-optic modulation bandwidth corresponds to 6-dB roll-off in the microwave transmission S_{21}, which exceeds 300 GHz for a device with 10 mm modulation length. The microwave reflection S_{11} remains below –20 dB up to 300 GHz, indicating satisfactory impedance matching.

Optics EXPRESS

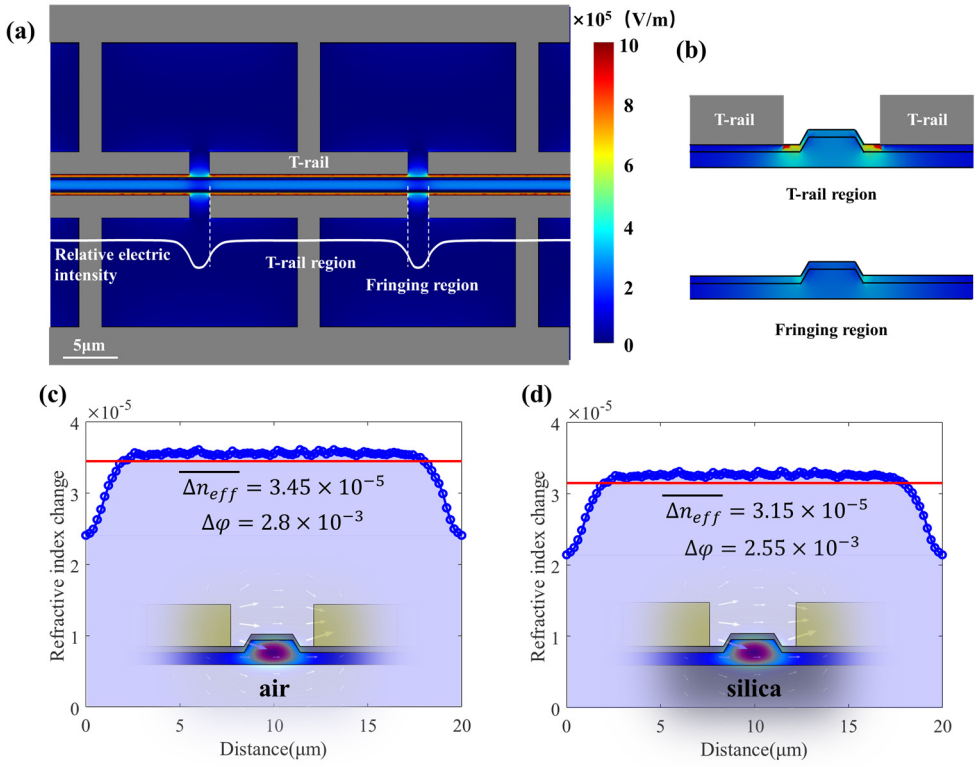

Fig. 6. (a) Electric field distribution between the electrode gap (top view). The averaged electric field along the optical waveguide is indicated by the white line. (b) Electric field distribution with and w/o T-rails on both sides (cross-section view). Refractive index variation along the optical waveguide with (c) BCB/air bonding layer and (d) silica bonding layer.

For a precise estimation of the electro-optic frequency response, the impedance and velocity mismatch as well as the microwave transmission loss are taken into account via a full-wave simulation [26]. As the length of the T-rail is much smaller than the microwave wavelength, the CL-TWEs can be modelled as lumped elements connected to the main electrodes. According to the transmission line model, the average effective loaded voltage along the modulation length L at modulation frequency ω can be expressed as [26]:

$$V_{avg}(\omega) = \frac{1}{L}\sum_{i=1}^{M}\frac{V_{\max}}{2}(1+\rho_1)e^{i\beta_o L}\frac{e^{i(\beta_e-\beta_o)(i-\frac{1}{2})L_p} + \rho_2 e^{-i(\beta_e+\beta_o)(i-\frac{1}{2})L_p}}{e^{i\beta_e L} + \rho_1\rho_2 e^{-i\beta_e L}}L_{act} \tag{7}$$

where M is the total number of T-rail electrodes, V_{max} is the amplitude of the driving voltage, L is the total length of the modulator, β_e-β_o and β_e+β_o represent the wave vector walk-off between the optical and the transmitted/reflected microwave signals, respectively, while ρ_1 and ρ_2 represent the input/output reflection coefficients of the microwave transmission line.

The electro-optic response of the proposed TFLN modulator with undercut structure is shown in Fig. 7(d). A 3-dB electro-optic bandwidth exceeding 300 GHz is predicted for a device with 10 mm modulation length.

Optics EXPRESS

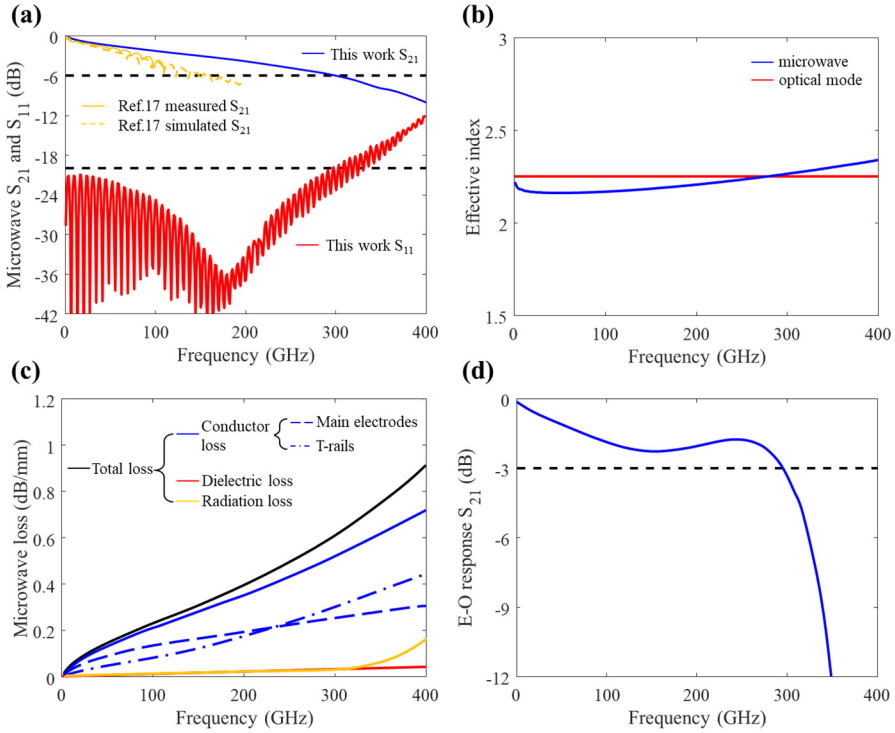

Fig. 7. (a) Microwave transmission S_{21} and reflection S_{11} for 10 mm modulation length. (b) Microwave refractive index and (c) microwave loss vs. frequency. (d) Electro-optic response for a modulator with 10 mm modulation length.

Table 2. Performance comparison of different modulator structure.

Structure	Ref.	$V_\pi \cdot L$	3-dB E-O bandwidth	V_π
CPW-TWEs	[6]	2.8 V·cm	45GHz @ 20mm	1.4 V
		2.3 V·cm	80GHz @ 10mm	2.3 V
		2.2 V·cm	100GHz @ 5mm	4.4 V
	[7]	2.5 V·cm	70GHz @ 5mm	5.1 V
	[8]	6.7 V·cm	106GHz @ 5mm	13 V
	[9]	3.7 V·cm	29GHz @ 24mm	1.3 V
	[10]	0.86 V·cm	>3GHz @ 7.5mm	1.15 V
	[11]	1.75 V·cm	>40GHz @ 5mm	3.5 V
CL-TWEs	[16]	2.6 V·cm	>50GHz @ 20mm (180 GHz predicted)	1.3 V
	[17]	1.7 V·cm	>67GHz @ 5mm (200 GHz predicted)	3.4 V
CL-TWEs (undercut structure)	This work	1.2 V·cm	300GHz @ 10 mm	1.2 V

4. Conclusions

A wideband TFLN modulator for sub-terahertz operation is proposed. With the undercut structure formed by partially-removed BCB bonding layer for velocity and impedance matching, both

Optics EXPRESS

ultra-wide bandwidth and low driving voltage can be realized simultaneously with narrow-gap CL-TWEs. For a device with 10-mm modulation length, half-wave voltage as low as 1.2 V can be obtained with narrow-gap (2 μm) and large-duty-cycle (90%) T-rails, while the 3-dB electro-optic bandwidth is estimated to be beyond 300 GHz. The performances of TFLN modulators based on different electrode and waveguide structures are summarized in Table 2.

The bandwidth-voltage limitation of TFLN modulators based on traditional CPW-TWEs is about 40 GHz/V, while value for devices with CL-TWEs is about 140 GHz/V. The proposed TFLN modulator based on an undercut structure is predicted to extend the limitation to 250 GHz/V, demonstrating the capacity for sub-terahertz operation with a low half-wave voltage.

Funding. National Key Research and Development Program of China (2018YFB2201701); National Natural Science Foundation of China (61822404, 61875104, 61904093, 61927811, 61974080, 61975093, 61991443); Key Lab Program of BNRist (BNR2019ZS01005); China Postdoctoral Science Foundation (2019T120090); Collaborative Innovation Centre of Solid-State Lighting and Energy-Saving Electronics.

Disclosures. The authors declare no conflicts of interest.

Data availability. Data underlying the results presented in this paper are not publicly available at this time but may be obtained from the authors upon reasonable request.

References

1. H. Murata, "Millimeter-Wave-Band Electro-Optic Modulators Using Antenna-Coupled Electrodes for Microwave Photonic Applications," J. Lightwave Technol. **38**(19), 5485–5491 (2020).
2. E. Li and A. X. Wang, "Theoretical Analysis of Energy Efficiency and Bandwidth Limit of Silicon Photonic Modulators," J. Lightwave Technol. **37**(23), 5801–5813 (2019).
3. Y. Ogiso, Y. Hashizume, H. Tanobe, N. Nunoya, M. Ida, Y. Miyamoto, M. Ishikawa, J. Ozaki, Y. Ueda, H. Wakita, M. Nagatani, H. Yamazaki, M. Nakamura, T. Kobayashi, and S. Kanazawa, "80-GHz Bandwidth and 1.5-V Vπ InP-Based IQ Modulator," J. Lightwave Technol. **38**(2), 249–255 (2020).
4. K. Noguchi, O. Mitomi, and H. Miyazawa, "Millimeter-wave Ti:$LiNbO_3$ optical modulators," J. Lightwave Technol. **16**(4), 615–619 (1998).
5. E. L. Wooten, K. M. Kissa, A. Yi-Yan, E. J. Murphy, D. A. Lafaw, P. F. Hallemeier, D. Maack, D. V. Attanasio, D. J. Fritz, G. J. McBrien, and D. E. Bossi, "A review of lithium niobate modulators for fiber-optic communications systems," IEEE J. Sel. Top. Quantum Electron. **6**(1), 69–82 (2000).
6. C. Wang, M. Zhang, X. Chen, M. Bertrand, A. Shams-Ansari, S. Chandrasekhar, P. Winzer, and M. Lončar, "Integrated lithium niobate electro-optic modulators operating at CMOS-compatible voltages," Nature **562**(7725), 101–104 (2018).
7. M. He, M. Xu, Y. Ren, J. Jian, Z. Ruan, Y. Xu, S. Gao, S. Sun, X. Wen, L. Zhou, L. Liu, C. Guo, H. Chen, S. Yu, L. Liu, and X. Cai, "High-performance hybrid silicon and lithium niobate Mach–Zehnder modulators for 100 Gbit s^{-1} and beyond," Nat. Photonics **13**(5), 359–364 (2019).
8. X. Wang, P. O. Weigel, J. Zhao, M. Ruesing, and S. Mookherjea, "Achieving beyond-100-GHz large-signal modulation bandwidth in hybrid silicon photonics Mach Zehnder modulators using thin film lithium niobate," APL Photonics **4**(9), 096101 (2019).
9. A. N. R. Ahmed, S. Shi, A. Mercante, N. Sean, Y. Peng, and W. P. Dennis, "High-efficiency lithium niobate modulator for K band operation," APL Photonics **5**(9), 091302 (2020).
10. M. Jin, J. Chen, Y. Sua, P. Kumar, and Y. Huang, "Efficient electro-optical modulation on thin-film lithium niobate," Opt. Lett. **46**(8), 1884–1887 (2021).
11. Y. Liu, H. Li, J. Liu, S. Tan, Q. Lu, and W. Guo, "Low Vπ thin-film lithium niobate modulator fabricated with photolithography," Opt. Express **29**(5), 6320–6329 (2021).
12. A. N. R. Ahmed, N. Sean, S. Shi, Y. Peng, A. Mercante, and W. P. Dennis, "Subvolt electro-optical modulator on thin-film lithium niobate and silicon nitride hybrid platform," Opt. Lett. **45**(5), 1112–1115 (2020).
13. R. Safian, M. Teng, L. Zhuang, and S. Chakravarty, "Foundry-compatible thin film lithium niobate modulator with RF electrodes buried inside the silicon oxide layer of the SOI wafer," Opt. Express **28**(18), 25843–25857 (2020).
14. S. Chakravarty, M. Teng, R. Safian, and L. Zhuang, "Hybrid material integration in silicon photonic integrated circuits," J. Semicond. **42**(4), 041303 (2021).
15. X. Liu, B. Xiong, C. Sun, Z. Hao, L. Wang, J. Wang, Y. Han, H. Li, J. Yu, and Y. Luo, "Low Half-wave-voltage Thin Film $LiNbO_3$ Electro-optic Modulator Based on a Compact Electrode Structure," in *Asia Communications and Photonics Conference* (Optical Society of America, 2020), paper M4A.144.
16. P. Kharel, C. Reimer, K. Luke, L. He, and M. Zhang, "Breaking voltage–bandwidth limits in integrated lithium niobate modulators using micro-structured electrodes," Optica **8**(3), 357–363 (2021).
17. X. Liu, B. Xiong, C. Sun, Z. Hao, L. Wang, J. Wang, Y. Han, H. Li, J. Yu, and Y. Luo, "Wideband thin-film lithium niobate modulator with low half-wave-voltage length product," Chin. Opt. Lett. **19**(6), 060016 (2021).
18. J. Shin, S. R. Sakamoto, and N. Dagli, "Conductor Loss of Capacitively Loaded Slow Wave Electrodes for High-Speed Photonic Devices," J. Lightwave Technol. **29**(1), 48–52 (2011).

Optics EXPRESS

19. H. Chen, "Development of an 80 Gbit/s InP-based Mach-Zehnder Modulator," Doctoral Thesis, Technischen Universität Berlin (2007).
20. S. Hähnle, N. Marrewijk, A. Endo, K. Karatsu, D. Thoen, V. Murugesan, and J. Baselmans, "Suppression of radiation loss in high kinetic inductance superconducting co-planar waveguides," Appl. Phys. Lett. **116**(18), 182601 (2020).
21. A. Vonsovici, R. Orobtchouk, and A. Koster, "Numerical simulation of a silicon-on-insulator waveguide Fabry-Perot interferometer for intensity light modulators at 1.3 μm," J. Lightwave Technol. **15**(11), 2124–2129 (1997).
22. T. K. Johansen, "EM simulation accuracy enhancement for broadband modeling of on-wafer passive components," in *2007 European Microwave Integrated Circuit Conference*, (IEEE, 2007), pp. 447–450.
23. J. A. Hejase, P. R. Paladhi, and P. P. Chahal, "Terahertz characterization of dielectric substrates for component design and nondestructive evaluation of packages," IEEE Trans. Compon., Packag., Manuf. Technol. **1**(11), 1685–1694 (2011).
24. A. Borgia and G. D. Massa, "Millimeter-Waves structures on benzocyclobutene dielectric substrate," Radioengineering. **20**, 785–789 (2011).
25. M. Lee, "Dielectric constant and loss tangent in $LiNbO_3$ crystals from 90 to 147 GHz,"," Appl. Phys. Lett. **79**(9), 1342–1344 (2001).
26. S. H. Lin and S.-Y. Wang, "High-throughput GaAs PIN electrooptic modulator with a 3-dB bandwidth of 9.6 GHz at 1.3 μm," Appl. Opt. **26**(9), 1696–1700 (1987).